

Digital logic from high-efficiency superconducting diodes

Pavan Hosur^{1,*}

¹Affiliation: Department of Physics and Texas Center for Superconductivity, University of Houston, Houston, TX 77204, USA

*phosur@uh.edu

ABSTRACT

Recent advancements in the realizations of superconducting diodes have pushed the diode coefficient η towards its theoretical maximum of $\eta = 1$. In this work, we describe the construction of logic gates NOT, AND, OR, NAND and NOR using superconducting diodes with $\eta \approx 1$ by exploiting their dynamically tunable polarity. We then argue that fundamental theorems suppress η in intrinsic superconductors, rendering them likely unsuitable for the proposed devices, and point out that several previous proposals and platforms, remarkably, bypassed this suppression unwittingly. We discuss the realization of the digital logic in one such platform – Josephson triodes that yielded $\eta \approx 1$ – and argue that phases with spontaneous spatial or magnetic order can overcome some of its drawbacks. Thus, this work provides guiding principles for future platforms and develops the building blocks for superconductors-based digital electronics.

1 Introduction

In recent years, the massive rise in global computational requirements has reinforced the need for low-cost, energy-efficient computing platforms. From this perspective, improvements in cryogenic cooling efficiencies and discoveries of superconductors in more accessible regimes of temperature and pressure inspire superconductors as a promising family of platforms. Moreover, superconductor-based classical computers would integrate naturally with superconducting quantum processors, where cryogenic classical logic has been identified as a potential solution to key challenges in scaling quantum computers, such as latency due to communication between classical and quantum computers and heating [1]. So far, the superconducting platform that has been used most for classical computing consists of Josephson arrays, which are inherently hard to scale as they require magnetic fields. Some superconducting transistors have also been realized...

Following the historical development of semiconductors-based digital technology, an alternative natural starting point for its superconducting counterpart is superconducting diodes (SDs), a field that has seen an explosive resurgence of interest in recent years. SDs are defined by unequal critical current magnitudes I_c^\pm in opposite directions and are typically characterized by the diode quality factor $\eta = \frac{I_c^+ - I_c^-}{I_c^+ + I_c^-} \in [0, 1]$, whose value has risen rapidly from $\eta \sim 10^{-2}$ in Ref. [2] to, remarkably, $\eta \approx 1$ in a Josephson trijunction [3]. The SD effect has been observed in a myriad of platforms [2–34] and inspired a wealth of theoretical activity aimed at explaining, enhancing and harnessing SDs for practical purposes [35–79]. It relies on a simple underlying principle to achieve non-reciprocal behavior: broken time reversal, inversion, and any other spatial symmetries that equate “left” and “right”. Crucially, they offer a tremendous advantage over semiconductor diodes, namely, their polarity can be dynamically trained with external fields.

In this work, inspired by the trajectory of semiconductors-based digital technology, we define the building blocks for an analogous path based on SDs. We rely on two key experimental developments: platforms with $\eta \approx 1$ and robust control of SD polarity. We first describe a simple ON/OFF switch with stable memory. We build on this design to construct a universal set of elementary Boolean logic gates, including composite gates where the output of one level feeds the input of the next. These constructions form building blocks for complex integrated circuits based on SDs. We then show that in intrinsic SDs, the implicit smoothness in Ginzburg-Landau free energies combined with Bloch’s theorem that restricts equilibrium current densities in isolated systems in the thermodynamic limit prevents $\eta \rightarrow 1$. Thus, natural intrinsic routes to $\eta \approx 1$ involve proximity-induced superconductivity and small devices, two approaches that circumvent Bloch’s theorem’s restrictions in different ways. Alternately, one can use Josephson devices as they are far from the thermodynamic limit and not subject to the above restrictions. Thus, we estimate the required parameters for the Josephson triode where $\eta \approx 1$ and tunable polarity have been achieved already [3].

Input Ising variable	Input physical variable	Output voltage	Logical value
$m < 0$	$V_D \sim I_c^+ R \times O(\varepsilon, R/R_N)$ or $B < 0$	$\sim I_c^+ R \times O(\varepsilon, R/R_N)$	0
$m > 0$	$V_D \sim I_c^+ R$ or $B > 0$	$\sim I_c^+ R$	1

Table 1. Input and output variables and their corresponding to the logical states. Input can be any binary Ising field, denoted m here, while outputs are voltages. To develop circuits using SDs, the Ising input must be mapped to the binary voltage values that define the logical output. The appropriate regime for digital logical operation is $r \ll R \ll R_N$ and $\varepsilon \ll 1$.

2 Results

Our starting point is an approximation for the current-voltage (I - V) characteristics for the SD sketched in Fig. 1 in non-ideal and ideal limits. The polarity of the SD is controlled by an Ising variable $m = \pm$. Denoting the normal state resistance by R_N and a small internal resistance of the superconductor due to defects, inhomogeneity etc. by $r \ll R_N$, we assume

$$V_m = \begin{cases} I_c^m r + (I - I_c^m) R_N & I > I_c^m \\ I r & -I_c^{\bar{m}} < I < I_c^m \\ -I_c^{\bar{m}} r + (I + I_c^{\bar{m}}) R_N & I < -I_c^{\bar{m}} \end{cases} \quad (1)$$

We emphasize three features of this I - V relationship that rely on the separation of scales, $I_c^+ \gg I_c^-$ and $R_N \gg r$: (i) in the supertransport regime, $-I_c^- < |I| < I_c^+$ near $V = 0$, I changes by a large, $O(1)$, amount for small, $O(\varepsilon)$, voltage change; (ii) I is nearly independent of V in the normal regimes, $|I| > I_c^+$. (iii) the I - V curve depends on m only through $\text{sgn}(m)$; it has no dependence on $|m|$, which is a fair assumption if the polarity stems from spontaneous order such as ferromagnetism or ferroelectricity whose moment has been saturated by the training field. The precise I - V relationship is immaterial if the above salient conditions are satisfied. For instance, nonreciprocal effects in the normal state, such as magnetochiral anisotropy, could be significant when $\varepsilon \ll 1$ in the SD. Nonetheless, as we show in App. A, the digital behaviors described in this work are robust in a parametrically large regime.

2.1 SD-based switch

To convert the SD into a switch, we exploit the fact that m can be reversed with an external field. For a fixed, external bias V in the interval $I_c^+ r \lesssim V \ll I_c^+ R_N$, the ON/OFF currents are defined as:

$$I \approx \begin{cases} I_c^+ (\text{ON}) & m < 0 \\ \varepsilon I_c^+ (\text{OFF}) & m > 0 \end{cases} \text{ if } I_c^+ r \lesssim V \ll I_c^+ R_N \quad (2)$$

where we have neglected subleading terms in ε and r/R_N . Note that using an external field to tune the current between I_c^+ and I_c^- or reverse its direction is routine for SDs. The novelties of the above result are the binary ON/OFF definitions and robustness afforded by the separation of scales between I_c^+ and I_c^- and between r and R_N . The upshot is that the ON/OFF states defined above are insensitive to the precise value of V as long as it is in the right range. This will allow us to precisely define Boolean logical states and construct universal gates below. We assumed $V > 0$ in this discussion, but the situation is identical for $V < 0$. Then, the appropriate range of V is $-I_c^+ R_N \ll V \lesssim -I_c^+ r$ while the binary states are $I \approx -I_c^+$ (ON) and $I \approx -\varepsilon I_c^+$ (OFF).

In Fig. 2, we introduce a circuit symbol for an ideal SD-based switch, which must be read as follows. The field that trains m – such as an out-of-plane (in-plane) displacement (magnetic) field in 2D systems with out-of-plane polarization (in-plane magnetization) – is applied along the shorter side of the rectangle while current flows along the longer side. The diagonal double-headed arrow depicts the biasing conditions. Specifically, a rightward or positive (leftward or negative) m yields a SD whose polarity is upward (downward).

2.2 Single-input NOT gate

To construct Boolean logic gates using the SD, we first introduce a load resistance R that satisfies $r \ll R \ll R_N$. Then, we define logical states as given in Table 1. Intuitively, large and small voltages $-O(1)$ and $O(\varepsilon, R/R_N)$, respectively – are defined as logical 1 and 0. For the Ising variable m , we arbitrarily choose $m < 0$ ($m > 0$) as logical 0 (1).

Secondly, to build digital circuits where the outputs at one layer of gates serve as inputs to the next layer, $\text{sgn}(m)$ must ultimately be electrically trainable. If m denotes magnetization, a magneto-electric or an electromagnet would be additionally needed to convert between electric and magnetic signals. In either case, we require that m is saturated by a voltage of $O(I_c^+ R)$; specifically, by $\pm I_c^+ R/2$ as we will see shortly. We will assume I_c^+ to be large enough that $\pm I_c^+ R/2$ can train $\text{sgn}(m)$ reliably. Note, R cannot be made too large as it is limited by R_N and Ohmic heating must be avoided as the devices are based on a SDs.

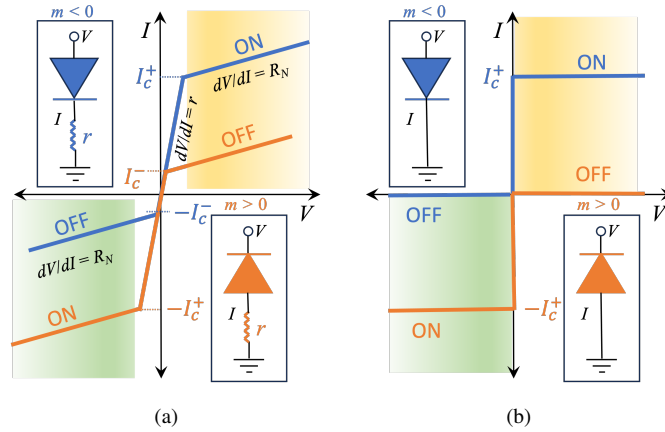


Figure 1. Schematic I - V characteristics of a highly efficient SD trainable by an external Ising field m in non-ideal (a) and ideal (b) limits. The yellow and green shaded regions offer separate digital switches that can be turned ON/OFF using m . Insets depict the effective SDs for each $\text{sgn}(m)$ with a small internal resistance r . Effective functionality requires $r \ll R_N$ and $\epsilon = I_c^- / I_c^+ \ll 1$. The ideal limit is defined by $r = 0$, $R_N \rightarrow \infty$ and $\epsilon = 0$.

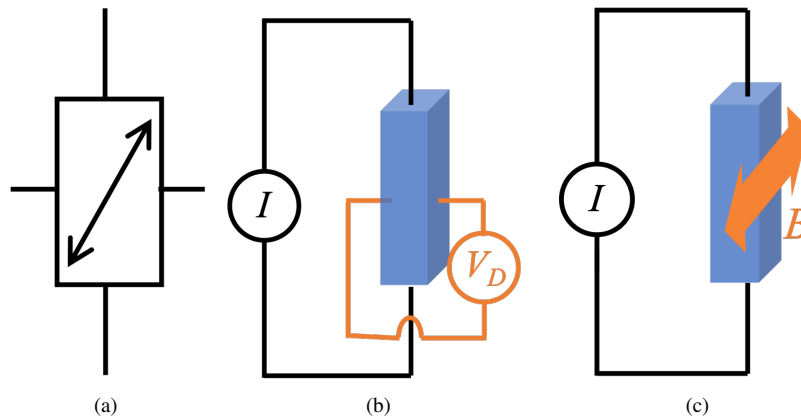


Figure 2. (a) Circuit symbol for the switch. The field that trains the SD polarity is along the width while transport is along the length. Rightward (leftward) training field yields a SD that superconducts for downward (upward) current and is Ohmic for the opposite current direction. (b,c) Illustration of the switch realized in a quasi-1D structure that exhibits (b) ferroelectricity trainable by the displacement voltage V_D or (c) ferromagnetism trainable by a magnetic field B . In most realizations, the current, displacement field, and magnetic field are mutually perpendicular.

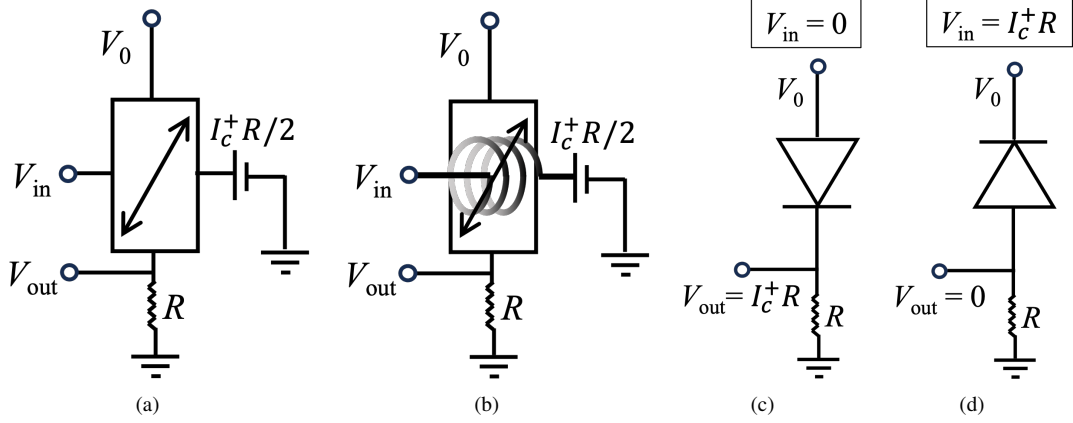


Figure 3. The NOT gate constructed from a high-efficiency SD whose polarity controlled by (a) an electric or (b) a magnetic field, and its effective diode depictions for input 0 (c) and input 1 (d). The double-headed arrow indicates the relationship between the diode polarity and the training field as in Fig. 2. Digital operation requires $I_c^+ R_N \gg V_0 > I_c^+ R$.

The definitions above immediately yield the simplest logic gate, the single bit NOT gate, shown in Fig. 3. In the presence of a bias voltage V_0 as shown, the input and output voltages in Fig. 3(a) can be straightforwardly be shown to satisfy the following exact relations assuming Eq. (1) (see App. B for details):

$$V_{\text{out}} = \begin{cases} \frac{V_0 + I_c^+ (R_N - r)}{R + R_N} R & V_{\text{in}} < I_c^+ R/2 \\ \frac{V_0 + I_c^- (R_N - r)}{R + R_N} R & V_{\text{in}} > I_c^+ R/2 \end{cases} \quad (3)$$

To first order in $1/R_N$ and ϵ , these expressions simplify to

$$V_{\text{out}} \approx \begin{cases} I_c^+ R \left(1 + \frac{V_0 / I_c^+ - R - r}{R_N} \right) \equiv 1 & V_{\text{in}} \equiv 0 \\ \epsilon I_c^+ R + V_0 \frac{R}{R_N} \equiv 0 & V_{\text{in}} \equiv 1 \end{cases} \quad (4)$$

where $V_{\text{in}} \equiv 0$ and 1 correspond to the ranges $V_{\text{in}} < I_c^+ R/2$ and $V_{\text{in}} > I_c^+ R/2$ and denote the appropriate logical values per the definitions in Table 1. Thus, setting V_0 in the range $I_c^+ (R + r) \lesssim V_0 \ll I_c^+ R_N$ turns the switch into a NOT gate whose 1 (0) output corresponds to the ON (OFF) states of the switch. In App. A, we show that including nonreciprocal effects in the normal state, quantified by a coefficient α with units of inverse current, merely raises the lower limit on V_0 to $\sim I_c^+ (R + r) / (1 - I_c^+ |\alpha|)$.

Intuitively, $V_{\text{in}} \approx 0$ makes the SD forward-biased and drives a large downward current $\sim I_c^+$, ensuring a large $V_{\text{out}} \approx I_c^+ R$ which corresponds to a logical 1. If $V_{\text{in}} \approx I_c^+ R$ on the other hand, the SD is reverse-biased, the downward current is $\sim \epsilon I_c^- + V_0 / R_N$ and $V_{\text{out}} \approx (\epsilon I_c^- + V_0 / R_N) R$ is correspondingly small, representing logical 0.

2.3 Two-input gates

Unlike semiconductor transistors and diodes, the current through the SD in the operating regime is fixed at I_c^+ or 0 to zeroth order in $1/R_N$ and ϵ . This restricts the allowed combinations of SDs and prevents, for instance, creating an OR gate by connecting inputs in parallel as is standard for semiconductor transistor-based gates. We now illustrate the design for the two-input gates NOR, AND, OR and NAND. Since all digital circuits can in principle be constructed from NOR or NAND, this section enables the leap from SD-based binary logic to digital computing in this platform.

A similar analysis as that performed for NOT allows the construction of the NOR and the AND gates, see Fig. 4(a,b). For brevity, we have only shown constructions based on electrically controllable SDs. Now, the inputs and outputs are related as

$$V_{\text{out}}^{\text{NOR}} \approx \begin{cases} I_c^+ R \left(1 + \frac{V_0 / I_c^+ - R - 2r}{2R_N} \right) & V_{\text{in}} \equiv 0, 0 \\ \epsilon I_c^+ R + V_0 \frac{R}{R_N} & V_{\text{in}} \equiv 0, 1 \\ \epsilon I_c^+ R + V_0 \frac{R}{R_N} & V_{\text{in}} \equiv 1, 0 \\ \epsilon I_c^+ R + V_0 \frac{R}{2R_N} & V_{\text{in}} \equiv 1, 1 \end{cases} \quad (5)$$

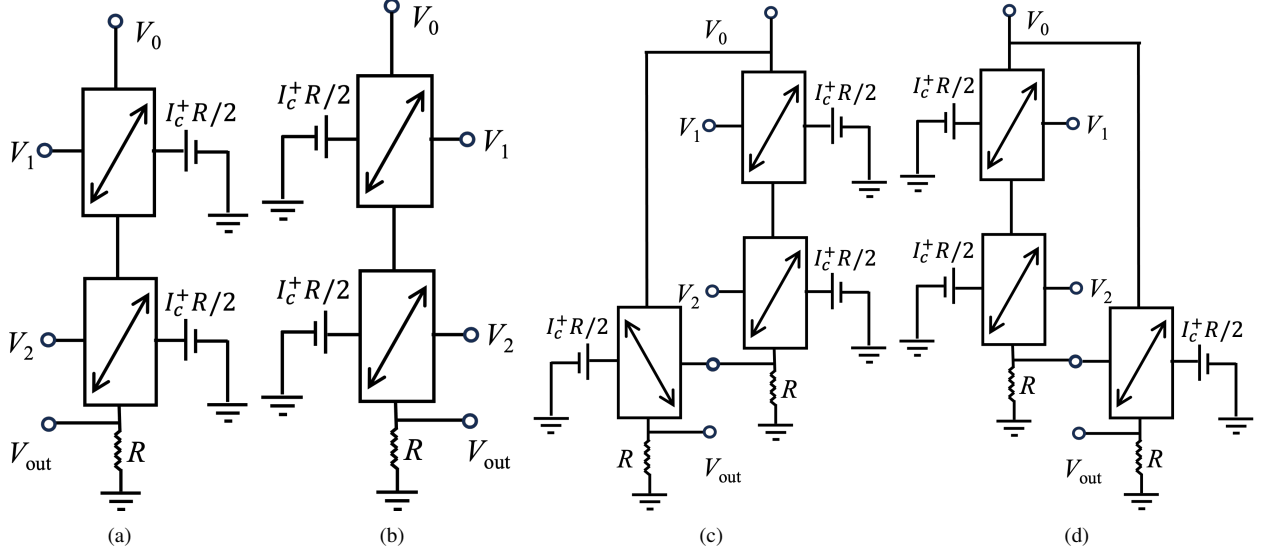


Figure 4. Two-input gates. (a) NOR (b) AND (c) OR (d) NAND. Negating the inputs of NOR (a) and NAND (c) with a NOT yield AND (b) and NAND (d), respectively, and vice-versa. Appending a NOT at the output of NOR (a) and AND (b) yields OR (c) and NAND (d), respectively.

where $V_{in} \equiv 0,0$ denotes $V_1 < I_c^+ R/2$, $V_2 < I_c^+ R/2$, etc. For the AND gate, the corresponding relations follow by reversing all the inequalities for V_{in} , since AND is equivalent to NOR with all the inputs negated:

$$V_{out}^{AND} \approx \begin{cases} I_c^+ R \left(1 + \frac{V_0/2I_c^+ - R/2 - r}{R_N} \right) & V_{in} \equiv 1, 1 \\ \varepsilon I_c^+ R + V_0 \frac{R}{R_N} & V_{in} \equiv 1, 0 \\ \varepsilon I_c^+ R + V_0 \frac{R}{R_N} & V_{in} \equiv 0, 1 \\ \varepsilon I_c^+ R + V_0 \frac{R}{2R_N} & V_{in} \equiv 0, 0 \end{cases} \quad (6)$$

Negating the outputs of NOR and AND yield OR and NAND, respectively, as shown in Figs. 4(c,d). In these cases, negation requires explicitly appending a NOT at the output. This is safe as long as the current through the transverse terminals is negligible or absent. Since NOR and NAND are universal gates, any digital circuit can be built in principle using SDs. Detailed analysis of all the gates is given in App. B.

3 Discussion

3.1 Barrier to $\varepsilon \ll 1$

Our results rely fundamentally on the condition $\varepsilon = I_c^- / I_c^+ \ll 1$, i.e., a low OFF/ON ratio, resulting in a small leakage current. However, we now show that basic principles hinder a small ε in intrinsic SDs.

Intrinsic SDs are typically described in theory by a Cooper pair momentum (q) dependent condensation energy density $F[q]$. Superconductivity exists only if $F[q] < 0$, and supercurrent density is given by $j(q) = 2e\partial_q F[q]$ whose largest positive and negative values in opposite directions are the critical current densities j_c^\pm . This approach is convenient in theory as it follows directly from a Bogoliubov-deGennes Hamiltonian that includes q -dependent pairing. However, it overlooks the fact that experiments invariably control j , not q .

Instead, consider the Gibbs condensation energy

$$G[j] = F[q(j)] - \frac{1}{2e} j q(j) \quad (7)$$

Again, superconductivity exists only when $G[j] < 0$. A fundamental theorem by Bloch forbids equilibrium current densities in arbitrary isolated quantum systems [80]. This mandates a stable equilibrium state at $j = 0$, corresponding to the conditions $G'[0] = 0$, $G''[0] > 0$. Moreover, $G[0] < 0$ for this state to be superconducting while j_c^\pm are magnitudes of the smallest positive and negative roots of $G[j]$, which implies $G[j_c^\pm] = 0$. The upshot of these conditions is that a large η or small ε , defined by

$j_c^\pm \gg j_c^-$, requires $G[j]$ to change sharply around $j = 0$. In particular, the limit $\eta = 1$ requires $j_c^- = 0$ and $j_c^+ \neq 0$, which is inconsistent with $G[0] < 0$ unless $G[j]$ is non-analytic at $j = 0$, implying a phase transition distinct from the superconducting transition at $j = 0$. Indeed, Ref. [35] and [77] showed that $\eta = 1$ at a tricritical point in superconducting Rashba metals and along a critical line in superconducting altermagnets, respectively. However, these proposals require fine-tuning to criticality and motivate a search for alternatives.

3.2 Experimental platforms with large η

One such route is through the proximity effect, which offers the added advantage of providing a natural substrate for patterning the desired circuit. Refs. [76, 81] exploited this effect to propose routes to $\eta = 1$ on superconductor surfaces without fine-tuning. On the experimental front, nanowires of superconducting β -Sn were recently patterned on the surface of the Dirac semimetal α -Sn [34]. The wires showed a large SD effect with a relatively $\eta \sim 25\%$ trainable by a longitudinal magnetic field. Moreover, the effect was argued to arise from the interface between the nanowires and the semimetal. In this setup, Bloch's theorem constrains the whole system, not the nanowire or the interface separately. Thus, $G'_{\text{wire}}[0]$ can be non-zero, allowing $j_c^\pm \gg j_c^-$ without $G_{\text{wire}}[j]$ relinquishing its analyticity.

Another route to a large η is via relatively small devices. This is because Bloch's theorem bounds the equilibrium current density by the inverse longitudinal dimension of the system [80], so short systems can carry non-negligible equilibrium currents. This idea likely helped reach $\eta \sim 65\%$ in heterostructures of ferromagnetic EuS and superconducting V deposited on Pt [9]. Here, asymmetries in the sample edges were key to obtaining a large SD effect, suggesting the importance of finite system size. This platform was further developed into multi-SD circuits for full wave rectification with $\sim 43\%$ efficiency and ac-to-dc conversion up to 40kHz [82].

Among existing platforms, arguably a strong candidate for realizing the proposals in this work is the Josephson triode made of MoRe-graphene-MoRe Josephson junctions [3]. Here, the microscopic physics is likely highly quantized and beyond the thermodynamic considerations of Ginzburg-Landau theory, such as the smoothness of free energy. In this device, a diode effect between two terminals was controlled by the current through a third terminal. Crucially, a representative device achieved $\eta \approx 1$ with $I_c^+ \approx 0.30 \mu\text{A}$ and training current $I_t \approx 0.16 \mu\text{A}$, while r was negligible compared to $R_N \approx 200 \Omega$. For these parameters, the designs we propose require $R \ll 200 \Omega$ and $V_0 \gtrsim I_c^+ R \sim 60 \mu\text{V}$, which are easily attainable. On the other hand, the Josephson triode has important drawbacks that hinder its scalability for digital circuits. In particular, I_t is comparable to the ON current I_c^+ and can lead to significant stray currents, unlike semiconductor transistor-based circuits where the bias current is negligible compared to the ON current. In addition, I_c^+ varies smoothly with I_t , making it vulnerable to noise in I_t .

For immunity against such noise, one would like the training field to couple to and saturate the order parameter of a spontaneously broken symmetry. In particular, a ferroelectric superconductor with additional time-reversal symmetry breaking would form an ideal platform, since it would allow electric control of SD polarity and the voltage output of one circuit layer can directly feed the input of the next. Electrostatic control of SD was recently achieved in Josephson diodes made of epitaxial Al-InAs junctions [83], but the control knob was a gate voltage on which I_c^+ depends smoothly and will presumably inherit noise from as in the Josephson triode. On the other hand, Ref. [43] proposed a SD based on a ferroelectric metal, bilayer NbSe₂ intercalated with Cu. Such metals were predicted in 1965 [84] but had been elusive until the recent discoveries of ferroelectricity in WTe₂ [85, 86] and bilayer graphene/boron nitride moire systems [87]. Recently, coupling between ferroelectricity and superconductivity was observed in bilayer MoTe₂ [88] while simultaneous ferromagnetism and electric polarity were seen for the first time in a metal, (Fe_{0.5}Co_{0.5})₅GeTe₂ [89], raising prospects of intrinsic or proximity-induced superconductivity in it to create a SD that is robustly trainable by both electric and magnetic fields. Along with the logic and designs described in this work, the above developments lay the groundwork and motivate a search for platforms for superconducting digital electronics.

4 Conclusions

We have tackled two key problems on the road to superconducting digital technology. First, we constructed circuits for logic gates based on high-efficiency SDs using only resistors and voltage sources. The key property of SDs that we exploit is their dynamically reversible polarity. We explicitly constructed NOT, AND, OR, NAND and NOR gates, thus providing several sets of universal building blocks for digital computing. Secondly, we discussed how fundamental principles reduce SD efficiency in intrinsic systems, thereby narrowing the search space of platforms where high efficiency is possible, and point out how an implicit circumvention of these principles led to high efficiency in some existing platforms. The proposed digital properties should be achievable in MoRe-graphene-MoRe Josephson triodes [3]; while scalable circuits will likely need trainable broken symmetry phases such as ferroelectrics and ferromagnets. In sum, this work paves the way for digital technology using superconducting diodes.

Acknowledgements

We thank Ramamoorthy Ramesh, Gururaj Naik, Ashvin Vishwanath, Nandini Trivedi, and Pedram Roushan for useful discussions. We are grateful to the Department of Physics and Astronomy, Rice University, and the Max Planck Institute for the Physics of Complex Systems for their hospitality during different parts of this project. This research was supported by the Department of Energy Basic Energy Sciences grant no. DE-SC0022264.

Appendix

A Effect of normal state rectification

Unless time-reversal, inversion, and appropriate spatial symmetries are broken only in the superconducting state, systems that exhibit a SD effect also perform rectification in the normal state. In other words, their normal state resistance is current dependent which in the simplest case can be written as:

$$R_N(I) \equiv \frac{dV}{dI} = R_0(1 + \alpha I) \quad (8)$$

A well-known example of such an effect is magnetochiral anisotropy where $\alpha I \equiv (\boldsymbol{\gamma} \times \mathbf{B}) \cdot \mathbf{I}$, \mathbf{B} being an external magnetic field and $\boldsymbol{\gamma}$ known as the magnetochiral anisotropy coefficient. Normal state rectification relies on the same symmetries as the SD effect, so it is conceivable that it would be significant in systems where the latter is highly efficient, i.e., $\varepsilon \ll 1$. On the other hand, it is also known that the ratio of $\boldsymbol{\gamma}$'s in the fluctuating-superconductor and normal regimes scales as [90]

$$\frac{\gamma_{SC}}{\gamma_N} \sim \left(\frac{E_F}{k_B T_c} \right)^3 \quad (9)$$

where E_F is the normal state Fermi energy and T_c is the superconducting transition temperature. As a result, it can grow by several orders of magnitude as superconductivity onsets [31, 32]. Thus, a small value of $|\alpha| \equiv |\boldsymbol{\gamma} \mathbf{B}|$, a normal state property, is physically consistent a large diode effect, $\eta \sim 1$ or $\varepsilon \ll 1$.

We now explicitly re-derive the characteristics of the NOT gate and prove that its digital behavior is robust as long as $|\alpha| \ll 1/I_c^+$. The basic I - V characteristics of the SD, including the resistance non-linearity, read:

$$V_m = \begin{cases} I_c^m r + (I - I_c^m) R_N(I) & I > I_c^m \\ I r & -I_c^{\bar{m}} < I < I_c^m \\ -I_c^{\bar{m}} r + (I + I_c^{\bar{m}}) R_N(I) & I < -I_c^{\bar{m}} \end{cases} \quad (10)$$

while the NOT gate characteristics become

$$V_0 = IR + I_c^+ r + (I - I_c^+) R_N(I) \text{ if } V_{in} < I_c^+ R/2 \text{ and } V_0 - IR > I_c^+ r \quad (11)$$

$$V_0 = IR + I_c^- r + (I - I_c^-) R_N(I) \text{ if } V_{in} > I_c^- R/2 \text{ and } V_0 - IR > I_c^- r \quad (12)$$

Solving for I ,

$$I = \frac{-[R + R_0(1 - I_c^\pm \alpha)] + \sqrt{[R + R_0(1 - I_c^\pm \alpha)]^2 + 4R_0\alpha [I_c^\pm (R_0 - r) + V_0]}}{2R_0\alpha} \quad (13)$$

for $V_0 - IR > I_c^\pm r$, where we have selected the root of the quadratic equation that is smoothly connected to the solution in the $\alpha \rightarrow 0$ limit. For $R_0 \gg R$ and $|\alpha| I_c^\pm \ll 1$, this simplifies to

$$I \approx \frac{I_c^\pm R_0 + V_0}{R_0(1 - I_c^\pm \alpha)} \quad (14)$$

Self-consistency requires $V_0 - IR > I_c^\pm r$ or

$$V_0 \gtrsim \frac{I_c^\pm R}{1 - I_c^\pm \alpha} + I_c^\pm r \quad (15)$$

Thus, a larger bias voltage, $V_0 \gtrsim \frac{I_c^+ R}{1 - |\alpha| I_c^+} > I_c^+ R$ ensures that the digital operation of the NOT gate as described in this paper. The analysis above also establishes that the normal state non-linearity merely demands an enhanced V_0 without qualitatively changing the physics. Therefore, other logic gate operations should also be similarly robust.

(a)

V_{bias} using Kirchoff's voltage law	Input voltages	Self-consistency condition	Physical state of SD1, SD2
$2[I_c^+ r + (I - I_c^+) R_N] + IR$	$V_1 < I_c^+ R/2, V_2 < I_c^+ R/2$	$I > I_c^+$	Normal, Normal
$Ir + I_c^- r + (I - I_c^-) R_N + I_c^- r + IR$	$V_1 < I_c^+ R/2, V_2 > I_c^+ R/2$	$I_c^- < I < I_c^+$	Superconducting, Normal
$I_c^- r + (I - I_c^-) R_N + I_c^- r + Ir + IR$	$V_1 > I_c^+ R/2, V_2 < I_c^+ R/2$	$I_c^- < I < I_c^+$	Normal, Superconducting
$2[I_c^- r + (I - I_c^-) R_N] + IR$	$V_1 > I_c^+ R/2, V_2 > I_c^+ R/2$	$I_c^- < I < I_c^+$	Normal, Normal

(b)

V_{bias} using Kirchoff's voltage law	Input voltages	Self-consistency condition	Physical state of SD1, SD2
$2[I_c^+ r + (I - I_c^+) R_N] + IR$	$V_1 > I_c^+ R/2, V_2 > I_c^+ R/2$	$I > I_c^+$	Normal, Normal
$Ir + I_c^- r + (I - I_c^-) R_N + I_c^- r + IR$	$V_1 > I_c^+ R/2, V_2 < I_c^+ R/2$	$I_c^- < I < I_c^+$	Superconducting, Normal
$I_c^- r + (I - I_c^-) R_N + I_c^- r + Ir + IR$	$V_1 < I_c^+ R/2, V_2 > I_c^+ R/2$	$I_c^- < I < I_c^+$	Normal, Superconducting
$2[I_c^- r + (I - I_c^-) R_N] + IR$	$V_1 < I_c^+ R/2, V_2 < I_c^+ R/2$	$I_c^- < I < I_c^+$	Normal, Normal

Table 2. Analysis of the (a) NOR and (b) AND gate circuits. SD1 and SD2 refer to the SDs receiving inputs V_1 and V_2 , respectively. For concreteness, we restrict to a regime where the voltage drop across each SD is positive, i.e., each SD is in the $V > 0$ region per Fig. 1. The precise regimes of each SD for various inputs are depicted below in Fig. 5.

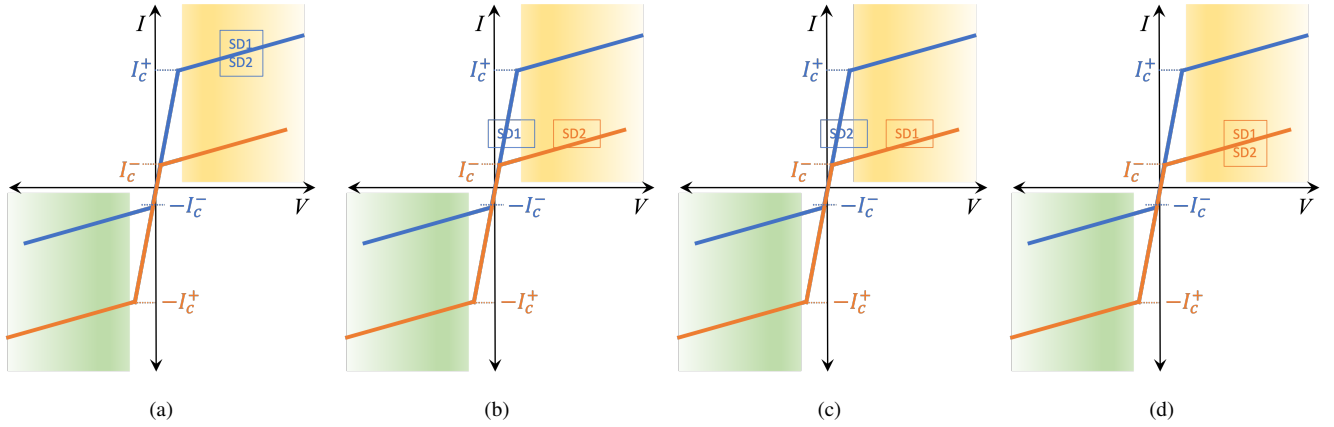


Figure 5. Illustration of the operating regime of the SDs receiving inputs V_1 and V_2 , denoted SD1 and SD2, respectively for the cases in each of Tables 1(a) and 1(b). Subfigures (a-d) correspond to rows (1-4) of the tables.

B Voltage relations for various gates

In this section, we supply the details that lead to the input-output voltage relations stated in the main text. The derivations are based Kirchoff's laws; the main departure from introductory physics is that Ohm's law is replaced by the SD I - V relation given in Eq. 1 of the main text.

Explicitly, for the single input NOT gate in Fig. 3, we have

$$V_0 = IR + I_c^+ r + (I - I_c^+) R_N \text{ if } V_{\text{in}} < I_c^+ R/2 \text{ and } V_0 - IR > I_c^+ r \quad (16)$$

$$V_0 = IR + I_c^- r + (I - I_c^-) R_N \text{ if } V_{\text{in}} > I_c^+ R/2 \text{ and } V_0 - IR > I_c^- r \quad (17)$$

where I is the downward current. Above, the condition on V_{in} implements the correct polarity of the SD while that on $V_0 - IR$ ensures self-consistency that the SD is in the assumed (normal) regime. With $V_{\text{out}} = IR$, this immediately yields Eq. (3) in the main text.

For the NOR and AND gates sketched in Fig. 4, the circuit analysis is summarized in Tables 1(a) and 1(b), respectively. Note that the only difference between the two tables occurs in column two, where all the inequalities are inverted. This reflects the simple logical fact that inverting the inputs of NOR yields AND and vice-versa. The physical states of the two SDs are indicated in Fig. 5.

References

1. Reilly, D. J. Challenges in Scaling-up the Control Interface of a Quantum Computer. *arXiv e-prints* arXiv:1912.05114, DOI: [10.48550/arXiv.1912.05114](https://doi.org/10.48550/arXiv.1912.05114) (2019). [1912.05114](https://doi.org/10.48550/arXiv.1912.05114).
2. Ando, F. *et al.* Observation of superconducting diode effect. *Nature* **584**, 373–376, DOI: [10.1038/s41586-020-2590-4](https://doi.org/10.1038/s41586-020-2590-4) (2020).
3. Chiles, J. *et al.* Nonreciprocal supercurrents in a field-free graphene josephson triode. *Nano Lett.* **23**, 5257–5263, DOI: [10.1021/acs.nanolett.3c01276](https://doi.org/10.1021/acs.nanolett.3c01276) (2023).
4. Jiang, X., Connolly, P. J., Hagen, S. J. & Lobb, C. J. Asymmetric current-voltage characteristics in type-ii superconductors. *Phys. Rev. B* **49**, 9244–9247, DOI: [10.1103/PhysRevB.49.9244](https://doi.org/10.1103/PhysRevB.49.9244) (1994).
5. Lyu, Y.-Y. *et al.* Superconducting diode effect via conformal-mapped nanoholes. *Nat. Commun.* **12**, 2703, DOI: [10.1038/s41467-021-23077-0](https://doi.org/10.1038/s41467-021-23077-0) (2021).
6. Du, W.-S. *et al.* Superconducting Diode Effect and Large Magnetochiral Anisotropy in T_d -MoTe₂ Thin Film. *arXiv e-prints* arXiv:2303.09052, DOI: [10.48550/arXiv.2303.09052](https://doi.org/10.48550/arXiv.2303.09052) (2023). [2303.09052](https://doi.org/10.48550/arXiv.2303.09052).
7. Sundaresh, A., Väyrynen, J. I., Lyanda-Geller, Y. & Rokhinson, L. P. Diamagnetic mechanism of critical current non-reciprocity in multilayered superconductors. *Nat. Commun.* **14**, 1628, DOI: [10.1038/s41467-023-36786-5](https://doi.org/10.1038/s41467-023-36786-5) (2023).
8. Kealhofer, R., Jeong, H., Rashidi, A., Balents, L. & Stemmer, S. Anomalous superconducting diode effect in a polar superconductor. *Phys. Rev. B* **107**, L100504, DOI: [10.1103/PhysRevB.107.L100504](https://doi.org/10.1103/PhysRevB.107.L100504) (2023).
9. Hou, Y. *et al.* Ubiquitous superconducting diode effect in superconductor thin films. *Phys. Rev. Lett.* **131**, 027001, DOI: [10.1103/PhysRevLett.131.027001](https://doi.org/10.1103/PhysRevLett.131.027001) (2023).
10. Chen, P. *et al.* Edelstein effect induced superconducting diode effect in inversion symmetry breaking mote2 josephson junctions. *Adv. Funct. Mater.* **34**, 2311229, DOI: <https://doi.org/10.1002/adfm.202311229> (2024).
11. Gupta, M. *et al.* Gate-tunable superconducting diode effect in a three-terminal josephson device. *Nat. Commun.* **14**, 3078, DOI: [10.1038/s41467-023-38856-0](https://doi.org/10.1038/s41467-023-38856-0) (2023).
12. Baumgartner, C. *et al.* Effect of rashba and dresselhaus spin–orbit coupling on supercurrent rectification and magnetochiral anisotropy of ballistic josephson junctions. *J. Physics: Condens. Matter* **34**, 154005, DOI: [10.1088/1361-648x/ac4d5e](https://doi.org/10.1088/1361-648x/ac4d5e) (2022).
13. Baumgartner, C. *et al.* Supercurrent rectification and magnetochiral effects in symmetric josephson junctions. *Nat. Nanotechnol.* **17**, 39–44, DOI: [10.1038/s41565-021-01009-9](https://doi.org/10.1038/s41565-021-01009-9) (2022).
14. Banerjee, A. *et al.* Phase asymmetry of andreev spectra from cooper-pair momentum. *Phys. Rev. Lett.* **131**, 196301, DOI: [10.1103/PhysRevLett.131.196301](https://doi.org/10.1103/PhysRevLett.131.196301) (2023).
15. Pal, B. *et al.* Josephson diode effect from cooper pair momentum in a topological semimetal. *Nat. Phys.* DOI: [10.1038/s41567-022-01699-5](https://doi.org/10.1038/s41567-022-01699-5) (2022).
16. Kim, J.-K. *et al.* Intrinsic supercurrent non-reciprocity coupled to the crystal structure of a van der Waals Josephson barrier. *Nat. Commun.* **15**, 1120, DOI: [10.1038/s41467-024-45298-9](https://doi.org/10.1038/s41467-024-45298-9) (2024). [2303.13049](https://doi.org/10.1038/s41467-024-45298-9).
17. Turini, B. *et al.* Josephson diode effect in high-mobility insb nanoflags. *Nano Lett.* **22**, 8502–8508, DOI: [10.1021/acs.nanolett.2c02899](https://doi.org/10.1021/acs.nanolett.2c02899) (2022).
18. Bauriedl, L. *et al.* Supercurrent diode effect and magnetochiral anisotropy in few-layer nbse2. *Nat. Commun.* **13**, 4266, DOI: [10.1038/s41467-022-31954-5](https://doi.org/10.1038/s41467-022-31954-5) (2022).
19. Wu, H. *et al.* The field-free josephson diode in a van der waals heterostructure. *Nature* **604**, 653–656, DOI: [10.1038/s41586-022-04504-8](https://doi.org/10.1038/s41586-022-04504-8) (2022).
20. Diez-Merida, J. *et al.* Magnetic josephson junctions and superconducting diodes in magic angle twisted bilayer graphene, DOI: [10.48550/ARXIV.2110.01067](https://doi.org/10.48550/ARXIV.2110.01067) (2021).

21. Golod, T. & Krasnov, V. M. Demonstration of a superconducting diode-with-memory, operational at zero magnetic field with switchable nonreciprocity. *Nat. Commun.* **13**, 3658, DOI: [10.1038/s41467-022-31256-w](https://doi.org/10.1038/s41467-022-31256-w) (2022).
22. Zhang, F. *et al.* Magnetic-field-free nonreciprocal transport in graphene multiterminal josephson junctions. *Phys. Rev. Appl.* **21**, 034011, DOI: [10.1103/PhysRevApplied.21.034011](https://doi.org/10.1103/PhysRevApplied.21.034011) (2024).
23. Yun, J. *et al.* Magnetic proximity-induced superconducting diode effect and infinite magnetoresistance in a van der waals heterostructure. *Phys. Rev. Res.* **5**, L022064, DOI: [10.1103/PhysRevResearch.5.L022064](https://doi.org/10.1103/PhysRevResearch.5.L022064) (2023).
24. Jeon, K.-R. *et al.* Zero-field polarity-reversible josephson supercurrent diodes enabled by a proximity-magnetized pt barrier. *Nat. Mater.* **21**, 1008–1013, DOI: [10.1038/s41563-022-01300-7](https://doi.org/10.1038/s41563-022-01300-7) (2022).
25. Lin, J.-X. *et al.* Zero-field superconducting diode effect in small-twist-angle trilayer graphene. *Nat. Phys.* **18**, 1221–1227, DOI: [10.1038/s41567-022-01700-1](https://doi.org/10.1038/s41567-022-01700-1) (2022).
26. Anwar, M. S. *et al.* Spontaneous superconducting diode effect in non-magnetic nb/ru/sr2ruo4 topological junctions. *Commun. Phys.* **6**, 290, DOI: [10.1038/s42005-023-01409-4](https://doi.org/10.1038/s42005-023-01409-4) (2023).
27. Narita, H. *et al.* Field-free superconducting diode effect in noncentrosymmetric superconductor/ferromagnet multilayers. *Nat. Nanotechnol.* **17**, 823–828, DOI: [10.1038/s41565-022-01159-4](https://doi.org/10.1038/s41565-022-01159-4) (2022).
28. Gutfreund, A. *et al.* Direct observation of a superconducting vortex diode. *Nat. Commun.* **14**, 1630, DOI: [10.1038/s41467-023-37294-2](https://doi.org/10.1038/s41467-023-37294-2) (2023).
29. Zhao, S. Y. F. *et al.* Time-reversal symmetry breaking superconductivity between twisted cuprate superconductors. *Science* **382**, 1422–1427, DOI: [10.1126/science.abl8371](https://doi.org/10.1126/science.abl8371) (2023). <https://www.science.org/doi/pdf/10.1126/science.abl8371>.
30. Trahms, M. *et al.* Diode effect in josephson junctions with a single magnetic atom. *Nature* **615**, 628–633, DOI: [10.1038/s41586-023-05743-z](https://doi.org/10.1038/s41586-023-05743-z) (2023).
31. Yasuda, K. *et al.* Nonreciprocal charge transport at topological insulator/superconductor interface. *Nat. Commun.* **10**, 2734, DOI: [10.1038/s41467-019-10658-3](https://doi.org/10.1038/s41467-019-10658-3) (2019).
32. Masuko, M. *et al.* Nonreciprocal charge transport in topological superconductor candidate bi2te3/pdte2 heterostructure. *npj Quantum Mater.* **7**, 104, DOI: [10.1038/s41535-022-00514-x](https://doi.org/10.1038/s41535-022-00514-x) (2022).
33. He, J. *et al.* Observation of superconducting diode effect in antiferromagnetic mott insulator α -rucl₃ (2024). [2409.04093](https://doi.org/10.26434/chemrxiv-2024-24093).
34. Anh, L. D. *et al.* Large superconducting diode effect in ion-beam patterned sn-based superconductor nanowire/topological dirac semimetal planar heterostructures. *Nat. Commun.* **15**, 8014, DOI: [10.1038/s41467-024-52080-4](https://doi.org/10.1038/s41467-024-52080-4) (2024).
35. Yuan, N. F. Q. & Fu, L. Supercurrent diode effect and finite-momentum superconductors. *Proc. Natl. Acad. Sci.* **119**, e2119548119, DOI: [10.1073/pnas.2119548119](https://doi.org/10.1073/pnas.2119548119) (2022). <https://www.pnas.org/doi/pdf/10.1073/pnas.2119548119>.
36. Daido, A., Ikeda, Y. & Yanase, Y. Intrinsic superconducting diode effect. *Phys. Rev. Lett.* **128**, 037001, DOI: [10.1103/PhysRevLett.128.037001](https://doi.org/10.1103/PhysRevLett.128.037001) (2022).
37. Daido, A. & Yanase, Y. Superconducting diode effect and nonreciprocal transition lines. *Phys. Rev. B* **106**, 205206, DOI: [10.1103/PhysRevB.106.205206](https://doi.org/10.1103/PhysRevB.106.205206) (2022).
38. Zhang, Y., Gu, Y., Li, P., Hu, J. & Jiang, K. General theory of josephson diodes. *Phys. Rev. X* **12**, 041013, DOI: [10.1103/PhysRevX.12.041013](https://doi.org/10.1103/PhysRevX.12.041013) (2022).
39. Davydova, M., Prembabu, S. & Fu, L. Universal josephson diode effect. *Sci. Adv.* **8**, eabo0309, DOI: [10.1126/sciadv.abo0309](https://doi.org/10.1126/sciadv.abo0309) (2022). <https://www.science.org/doi/pdf/10.1126/sciadv.abo0309>.
40. Chen, K., Karki, B. & Hosur, P. Intrinsic superconducting diode effects in tilted weyl and dirac semimetals. *Phys. Rev. B* **109**, 064511, DOI: [10.1103/PhysRevB.109.064511](https://doi.org/10.1103/PhysRevB.109.064511) (2024).
41. Wang, D., Wang, Q.-H. & Wu, C. Symmetry constraints on direct-current josephson diodes (2022). [2209.12646](https://doi.org/10.26434/chemrxiv-2022-12646).
42. He, J. J., Tanaka, Y. & Nagaosa, N. A phenomenological theory of superconductor diodes. *New J. Phys.* **24**, 053014, DOI: [10.1088/1367-2630/ac6766](https://doi.org/10.1088/1367-2630/ac6766) (2022).

43. Zhai, B., Li, B., Wen, Y., Wu, F. & He, J. Prediction of ferroelectric superconductors with reversible superconducting diode effect. *Phys. Rev. B* **106**, L140505, DOI: [10.1103/PhysRevB.106.L140505](https://doi.org/10.1103/PhysRevB.106.L140505) (2022).
44. Misaki, K. & Nagaosa, N. Theory of the nonreciprocal josephson effect. *Phys. Rev. B* **103**, 245302, DOI: [10.1103/PhysRevB.103.245302](https://doi.org/10.1103/PhysRevB.103.245302) (2021).
45. Ilić, S. & Bergeret, F. S. Theory of the supercurrent diode effect in rashba superconductors with arbitrary disorder. *Phys. Rev. Lett.* **128**, 177001, DOI: [10.1103/PhysRevLett.128.177001](https://doi.org/10.1103/PhysRevLett.128.177001) (2022).
46. Scammell, H. D., Li, J. I. A. & Scheurer, M. S. Theory of zero-field superconducting diode effect in twisted trilayer graphene. *2D Mater.* **9**, 025027, DOI: [10.1088/2053-1583/ac5b16](https://doi.org/10.1088/2053-1583/ac5b16) (2022).
47. Zinkl, B., Hamamoto, K. & Sigrist, M. Symmetry conditions for the superconducting diode effect in chiral superconductors. *Phys. Rev. Res.* **4**, 033167, DOI: [10.1103/PhysRevResearch.4.033167](https://doi.org/10.1103/PhysRevResearch.4.033167) (2022).
48. He, J. J., Tanaka, Y. & Nagaosa, N. The supercurrent diode effect and nonreciprocal paraconductivity due to the chiral structure of nanotubes. *Nat. Commun.* **14**, 3330, DOI: [10.1038/s41467-023-39083-3](https://doi.org/10.1038/s41467-023-39083-3) (2023).
49. Jiang, J. *et al.* Field-free superconducting diode in a magnetically nanostructured superconductor. *Phys. Rev. Appl.* **18**, 034064, DOI: [10.1103/PhysRevApplied.18.034064](https://doi.org/10.1103/PhysRevApplied.18.034064) (2022).
50. Kokkeler, T. H., Golubov, A. A. & Bergeret, F. S. Field-free anomalous junction and superconducting diode effect in spin-split superconductor/topological insulator junctions. *Phys. Rev. B* **106**, 214504, DOI: [10.1103/PhysRevB.106.214504](https://doi.org/10.1103/PhysRevB.106.214504) (2022).
51. Debnath, D. & Dutta, P. Gate-tunable josephson diode effect in rashba spin-orbit coupled quantum dot junctions. *Phys. Rev. B* **109**, 174511, DOI: [10.1103/PhysRevB.109.174511](https://doi.org/10.1103/PhysRevB.109.174511) (2024).
52. Chazono, M., Kanasugi, S., Kitamura, T. & Yanase, Y. Piezoelectric effect and diode effect in anapole and monopole superconductors. *Phys. Rev. B* **107**, 214512, DOI: [10.1103/PhysRevB.107.214512](https://doi.org/10.1103/PhysRevB.107.214512) (2023).
53. Vodolazov, D. Y. & Peeters, F. M. Superconducting rectifier based on the asymmetric surface barrier effect. *Phys. Rev. B* **72**, 172508, DOI: [10.1103/PhysRevB.72.172508](https://doi.org/10.1103/PhysRevB.72.172508) (2005).
54. de Picoli, T., Blood, Z., Lyanda-Geller, Y. & Väyrynen, J. I. Superconducting diode effect in quasi-one-dimensional systems. *Phys. Rev. B* **107**, 224518, DOI: [10.1103/PhysRevB.107.224518](https://doi.org/10.1103/PhysRevB.107.224518) (2023).
55. Kochan, D., Costa, A., Zhumagulov, I. & Žutić, I. Phenomenological Theory of the Supercurrent Diode Effect: The Lifshitz Invariant. *arXiv e-prints* arXiv:2303.11975, DOI: [10.48550/arXiv.2303.11975](https://doi.org/10.48550/arXiv.2303.11975) (2023). [2303.11975](https://arxiv.org/abs/2303.11975).
56. Ikeda, Y., Daido, A. & Yanase, Y. Intrinsic superconducting diode effect in disordered systems. *arXiv e-prints* arXiv:2212.09211, DOI: [10.48550/arXiv.2212.09211](https://doi.org/10.48550/arXiv.2212.09211) (2022). [2212.09211](https://arxiv.org/abs/2212.09211).
57. Tanaka, Y., Lu, B. & Nagaosa, N. Theory of giant diode effect in *d*-wave superconductor junctions on the surface of a topological insulator. *Phys. Rev. B* **106**, 214524, DOI: [10.1103/PhysRevB.106.214524](https://doi.org/10.1103/PhysRevB.106.214524) (2022).
58. Wang, D., Wang, Q.-H. & Wu, C. Symmetry Constraints on Direct-Current Josephson Diodes. *arXiv e-prints* arXiv:2209.12646, DOI: [10.48550/arXiv.2209.12646](https://doi.org/10.48550/arXiv.2209.12646) (2022). [2209.12646](https://arxiv.org/abs/2209.12646).
59. Haenel, R. & Can, O. Superconducting diode from flux biased Josephson junction arrays. *arXiv e-prints* arXiv:2212.02657, DOI: [10.48550/arXiv.2212.02657](https://doi.org/10.48550/arXiv.2212.02657) (2022). [2212.02657](https://arxiv.org/abs/2212.02657).
60. Legg, H. F., Laubscher, K., Loss, D. & Klinovaja, J. Parity-protected superconducting diode effect in topological josephson junctions. *Phys. Rev. B* **108**, 214520, DOI: [10.1103/PhysRevB.108.214520](https://doi.org/10.1103/PhysRevB.108.214520) (2023).
61. Cuzzo, J. J., Pan, W., Shabani, J. & Rossi, E. Microwave-tunable diode effect in asymmetric squids with topological josephson junctions. *Phys. Rev. Res.* **6**, 023011, DOI: [10.1103/PhysRevResearch.6.023011](https://doi.org/10.1103/PhysRevResearch.6.023011) (2024).
62. Souto, R. S., Leijnse, M. & Schrade, C. Josephson diode effect in supercurrent interferometers. *Phys. Rev. Lett.* **129**, 267702, DOI: [10.1103/PhysRevLett.129.267702](https://doi.org/10.1103/PhysRevLett.129.267702) (2022).
63. Seoane Souto, R. *et al.* Tuning the josephson diode response with an ac current. *Phys. Rev. Res.* **6**, L022002, DOI: [10.1103/PhysRevResearch.6.L022002](https://doi.org/10.1103/PhysRevResearch.6.L022002) (2024).

64. Cheng, Q. & Sun, Q.-F. Josephson diode based on conventional superconductors and a chiral quantum dot. *Phys. Rev. B* **107**, 184511, DOI: [10.1103/PhysRevB.107.184511](https://doi.org/10.1103/PhysRevB.107.184511) (2023).
65. Steiner, J. F., Melischek, L., Trahms, M., Franke, K. J. & von Oppen, F. Diode effects in current-biased josephson junctions. *Phys. Rev. Lett.* **130**, 177002, DOI: [10.1103/PhysRevLett.130.177002](https://doi.org/10.1103/PhysRevLett.130.177002) (2023).
66. Costa, A., Fabian, J. & Kochan, D. Microscopic study of the josephson supercurrent diode effect in josephson junctions based on two-dimensional electron gas. *Phys. Rev. B* **108**, 054522, DOI: [10.1103/PhysRevB.108.054522](https://doi.org/10.1103/PhysRevB.108.054522) (2023).
67. Wei, Y.-J., Liu, H.-L., Wang, J. & Liu, J.-F. Supercurrent rectification effect in graphene-based josephson junctions. *Phys. Rev. B* **106**, 165419, DOI: [10.1103/PhysRevB.106.165419](https://doi.org/10.1103/PhysRevB.106.165419) (2022).
68. Legg, H. F., Loss, D. & Klinovaja, J. Superconducting diode effect due to magnetochiral anisotropy in topological insulators and rashba nanowires. *Phys. Rev. B* **106**, 104501, DOI: [10.1103/PhysRevB.106.104501](https://doi.org/10.1103/PhysRevB.106.104501) (2022).
69. Karabassov, T., Bobkova, I. V., Golubov, A. A. & Vasenko, A. S. Hybrid helical state and superconducting diode effect in superconductor/ferromagnet/topological insulator heterostructures. *Phys. Rev. B* **106**, 224509, DOI: [10.1103/PhysRevB.106.224509](https://doi.org/10.1103/PhysRevB.106.224509) (2022).
70. Hu, J.-X., Sun, Z.-T., Xie, Y.-M. & Law, K. T. Josephson diode effect induced by valley polarization in twisted bilayer graphene. *Phys. Rev. Lett.* **130**, 266003, DOI: [10.1103/PhysRevLett.130.266003](https://doi.org/10.1103/PhysRevLett.130.266003) (2023).
71. Wu, Y.-M., Wu, Z. & Yao, H. Pair-density-wave and chiral superconductivity in twisted bilayer transition metal dichalcogenides. *Phys. Rev. Lett.* **130**, 126001, DOI: [10.1103/PhysRevLett.130.126001](https://doi.org/10.1103/PhysRevLett.130.126001) (2023).
72. Nunchot, N. & Yanase, Y. Chiral superconducting diode effect by dzyaloshinsky-moriya interaction. *Phys. Rev. B* **109**, 054508, DOI: [10.1103/PhysRevB.109.054508](https://doi.org/10.1103/PhysRevB.109.054508) (2024).
73. Daido, A. & Yanase, Y. Unidirectional Superconductivity and Diode Effect Induced by Dissipation. *arXiv e-prints* arXiv:2310.02539, DOI: [10.48550/arXiv.2310.02539](https://doi.org/10.48550/arXiv.2310.02539) (2023). [2310.02539](https://arxiv.org/abs/2310.02539).
74. Cayao, J., Nagaosa, N. & Tanaka, Y. Enhancing the josephson diode effect with majorana bound states. *Phys. Rev. B* **109**, L081405, DOI: [10.1103/PhysRevB.109.L081405](https://doi.org/10.1103/PhysRevB.109.L081405) (2024).
75. Banerjee, S. & Scheurer, M. S. Enhanced superconducting diode effect due to coexisting phases. *Phys. Rev. Lett.* **132**, 046003, DOI: [10.1103/PhysRevLett.132.046003](https://doi.org/10.1103/PhysRevLett.132.046003) (2024).
76. Hosur, P. & Palacios, D. Proximity-induced equilibrium supercurrent and perfect superconducting diode effect due to band asymmetry. *Phys. Rev. B* **108**, 094513, DOI: [10.1103/PhysRevB.108.094513](https://doi.org/10.1103/PhysRevB.108.094513) (2023).
77. Chakraborty, D. & Black-Schaffer, A. M. Perfect superconducting diode effect in altermagnets (2024). [2408.07747](https://arxiv.org/abs/2408.07747).
78. Soori, A. Josephson diode effect in one-dimensional quantum wires connected to superconductors with mixed singlet-triplet pairing. *arXiv e-prints* arXiv:2409.02794, DOI: [10.48550/arXiv.2409.02794](https://doi.org/10.48550/arXiv.2409.02794) (2024). [2409.02794](https://arxiv.org/abs/2409.02794).
79. Soori, A. Josephson diode effect in junctions of superconductors with band asymmetric metals. *J. Physics: Condens. Matter* **36**, 335303, DOI: [10.1088/1361-648X/ad4aad](https://doi.org/10.1088/1361-648X/ad4aad) (2024).
80. Watanabe, H. A proof of the bloch theorem for lattice models. *J. Stat. Phys.* **177**, 717–726, DOI: [10.1007/s10955-019-02386-1](https://doi.org/10.1007/s10955-019-02386-1) (2019).
81. Yuan, N. F. Q. Surface supercurrent diode effect (2023). [2305.04219](https://arxiv.org/abs/2305.04219).
82. Ingla-Aynés, J. *et al.* Highly Efficient Superconducting Diodes and Rectifiers for Quantum Circuitry. *arXiv e-prints* arXiv:2406.12012, DOI: [10.48550/arXiv.2406.12012](https://doi.org/10.48550/arXiv.2406.12012) (2024). [2406.12012](https://arxiv.org/abs/2406.12012).
83. Shin, J. *et al.* Electric control of polarity in spin-orbit josephson diode (2024). [2409.17820](https://arxiv.org/abs/2409.17820).
84. Anderson, P. W. & Blount, E. I. Symmetry considerations on martensitic transformations: "ferroelectric" metals? *Phys. Rev. Lett.* **14**, 217–219, DOI: [10.1103/PhysRevLett.14.217](https://doi.org/10.1103/PhysRevLett.14.217) (1965).
85. Fei, Z. *et al.* Ferroelectric switching of a two-dimensional metal. *Nature* **560**, 336–339, DOI: [10.1038/s41586-018-0336-3](https://doi.org/10.1038/s41586-018-0336-3) (2018).

86. de la Barrera, S. C. *et al.* Direct measurement of ferroelectric polarization in a tunable semimetal. *Nat. Commun.* **12**, 5298, DOI: [10.1038/s41467-021-25587-3](https://doi.org/10.1038/s41467-021-25587-3) (2021).
87. Zheng, Z. *et al.* Unconventional ferroelectricity in moiré heterostructures. *Nature* **588**, 71–76, DOI: [10.1038/s41586-020-2970-9](https://doi.org/10.1038/s41586-020-2970-9) (2020).
88. Jindal, A. *et al.* Coupled ferroelectricity and superconductivity in bilayer *td-mote2*. *Nature* **613**, 48–52, DOI: [10.1038/s41586-022-05521-3](https://doi.org/10.1038/s41586-022-05521-3) (2023).
89. Zhang, H. *et al.* A room temperature polar magnetic metal. *Phys. Rev. Mater.* **6**, 044403, DOI: [10.1103/PhysRevMaterials.6.044403](https://doi.org/10.1103/PhysRevMaterials.6.044403) (2022).
90. Wakatsuki, R. *et al.* Nonreciprocal charge transport in noncentrosymmetric superconductors. *Sci. Adv.* **3**, DOI: [10.1126/sciadv.1602390](https://doi.org/10.1126/sciadv.1602390) (2017).